ELSEVIER

Astroparticle Physics 10 (1999) 1–9

Astroparticle Physics

The EAS size spectrum and the cosmic ray energy spectrum in the region 10^{15}–10^{16} eV

EAS-TOP Collaboration

M. Aglietta [a,b], B. Alessandro [b], P. Antonioli [c], F. Arneodo [d], L. Bergamasco [b,e], M. Bertaina [b,e], C. Castagnoli [a,b], A. Castellina [a,b], A. Chiavassa [b,e], G. Cini Castagnoli [b,e], B. D'Ettorre Piazzoli [f], G. Di Sciascio [f], W. Fulgione [a,b], P. Galeotti [b,e], P.L. Ghia [a,b], M. Iacovacci [f], G. Mannocchi [a,b], C. Morello [a,b], G. Navarra [b,e,1], O. Saavedra [b,e], G.C. Trinchero [a,b], P. Vallania [a,b], S. Vernetto [a,b], C. Vigorito [a,b]

[a] *Istituto di Cosmo-Geofisica del CNR, Torino, Italy*
[b] *Istituto Nazionale di Fisica Nucleare, Sezione di Torino, Italy*
[c] *Istituto Nazionale di Fisica Nucleare, Sezione di Bologna, Italy*
[d] *Istituto Nazionale di Fisica Nucleare, Laboratori Nazionali del Gran Sasso, Assergi, L'Aquila, Italy*
[e] *Dipartimento di Fisica Generale dell'Università di Torino, Italy*
[f] *Dipartimento di Scienze Fisiche dell' Università di Napoli, and INFN, Sezione di Napoli, Italy*

Received 18 February 1998; accepted 31 July 1998

Abstract

The cosmic ray energy spectrum in the range $E_0 = 10^{15}$–10^{16} eV (including the region of the steepening, "*knee*") is studied by means of the EAS-TOP array (Campo Imperatore, Gran Sasso Laboratories, atmospheric depth 820 g cm^{-2}). Measurements of the electromagnetic size (N_e = total number of charged particles at the observation level) are performed as a function of zenith angle with statistical accuracies of a few percent. The change of slope of the spectrum is observed in each bin of zenith angle at size values decreasing with increasing atmospheric depth. Its attenuation is compatible with the one of shower particles ($\Lambda_e = 219 \pm 3$ g cm^{-2}). This observation provides a consistency check, supporting a normal behaviour of showers at the break, that make plausible astrophysical interpretations based on an effect on primaries occurring at a given primary energy. The break has a "*sharp*" shape (i.e., within experimental errors is compatible with two intersecting power laws) that represents a constraint with which any interpretation has to match. The change of slope of the power law index reproducing the size spectrum is $\Delta\gamma = 0.40 \pm 0.09$. The derived all particle energy spectrum is in good agreement with the extrapolation of the direct measurements at low energies and with other EAS data at and above the knee. Power laws fits to the energy spectrum below and above the knee give (in units of m^{-2} s^{-1} sr^{-1} TeV^{-1}) $S(E_0) = (3.48 \pm 0.06) \times 10^{-10}(E_0/2300)^{-2.76\pm0.03}$ for 900 TeV $< E_0 <$ 2300 TeV and $S(E_0) = (3.77 \pm 0.08) \times 10^{-11}(E_0/5000)^{-3.19\pm0.06}$ for 5000 TeV $< E_0 < 10^4$ TeV. The systematic uncertainties connected to the interaction model and the primary composition are discussed. © 1999 Elsevier Science B.V.

PACS: 96.40.De; 96.40.Pq
Keywords: Cosmic rays; Spectrum; Extensive Air Shower; EASTOP

PII S0927-6505(98)00035-8

1. Introduction

The measurement of the spectrum and composition of cosmic rays at high energies is still an open problem in High Energy Astrophysics, thus limiting the possibilities of setting a firm experimental basis to the problem of cosmic ray origin and propagation. This is particularly the case at primary energies $E_0 > 10^{15}$ eV, where, due to the low fluxes, $\Phi \approx 5 \times 10^{-2}$ particles$\cdot$m^{-2}sr^{-1} day^{-1}, the data have to be obtained through indirect measurements, i.e. the observation of Extensive Air Showers (EAS). But even the direct data obtained at lower energies by experiments operating on satellites or balloons suffer from statistical limitations and from methodological problems when measurements are not calorimetric.

The energy range $E_0 \approx 10^{15}$–10^{16} eV is of further interest since it is characterized by a break in the shower size spectrum [1], interpreted as a change in the cosmic ray primary energy spectrum ("knee"). Such "astrophysical" interpretation is now supported by observations of the break in the spectra of the electromagnetic [2–4], muon [3,4] and Cherenkov light [5,6] components of EAS. Different physical origins have been proposed for the interpretation of such break, leading to different predictions on the spectra of the different primary nuclei [7–10].

It is now important to perform measurements connecting the direct and the EAS experimental regions, and determine the characteristics of the break with good statistical accuracies, to derive its shape in energy and the possible corresponding changes of primary composition.

Moreover, at the energies of interest, we have no direct information on the hadronic cross sections for secondary production relevant for the interpretation of measurements. Extensive Air Showers experiments have therefore further to confirm that the "knee" itself is not due to a change of the hadronic physics, and provide a verification of the hadronic interaction models used to analyze the data.

From the experimental point of view, an exhaustive understanding of the problem requires the contemporaneous detection of the different EAS components in order to identify both the nature and the energy spectra of the primaries. Most of the information has been obtained, up to now, through the detection of the electromagnetic component that provides the measurement of the total number of ionizing particles (N_e = shower size, see Section 2). This technique has mainly contributed to the construction of the cosmic ray primary energy spectrum at high energies and to the observation of the quoted steepening.

The EAS-TOP experiment at Campo Imperatore (National Gran Sasso Laboratories) has been planned to perform complete observations of the atmospheric cascades through their different components (electromagnetic, muon, hadron, Cherenkov light, radio emission, with the further possibility of measuring in coincidence with experiments operating in the deep underground Gran Sasso laboratories, detecting the TeV muon content).

In this paper we present and discuss the results obtained in the study of the e.m. component (preliminary results were already presented in [3,11]), namely:

- the experimental data on the size spectrum around the knee;
- an analysis of the dependence of the parameters of the size spectra versus the atmospheric depth;
- the conversion of the size spectrum to the all particle energy spectrum;
- a comparison of the measured spectra with the extrapolations of the direct data.

2. The experiment and the analysis

The EAS-TOP array is located at Campo Imperatore, 2005 m a.s.l. (above the underground Gran Sasso laboratories), at 820 g cm^{-2} atmospheric depth. Its electromagnetic detector [12] is made of 35 scintillator modules, 10 m^2 each, separated by 20 m in the central region and 80 m at the edges of the array (see Fig. 1). In this work we will deal with four runs: run (I) with 29 active modules and runs (II)–(IV) with 35 modules in operation (each run covers about four months of data taking, with pressure variations $\sigma_p \sim 5$ g cm^{-2}). Each module is split into 16 individual scintillators (80×80 cm^2 area and 4 cm thickness); the accuracy in the particle density measurements is

$$\left(\frac{\sigma_\rho}{\rho}\right)^2 = \frac{\cos\theta + 0.02}{\rho} + \frac{0.038}{\sqrt{\rho}} + 0.042 \qquad (1)$$

[1] E-mail: NAVARRA@TO.INFN.IT

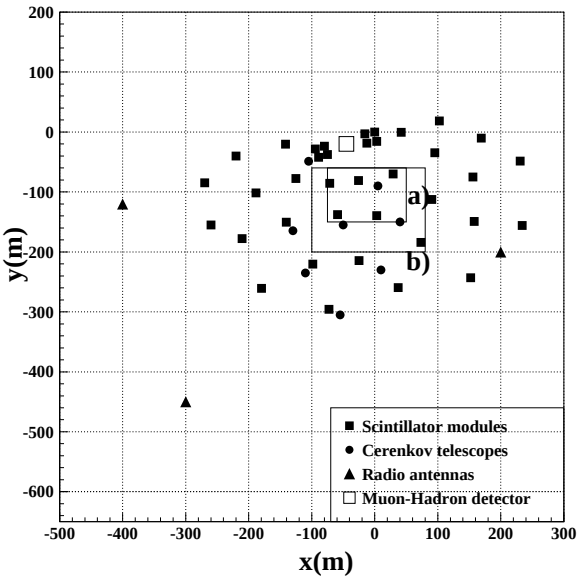

Fig. 1. The EAS-TOP array. (a) and (b) are the fiducial areas for the spectra measurements in run (I) and (II)–(IV), respectively (see text).

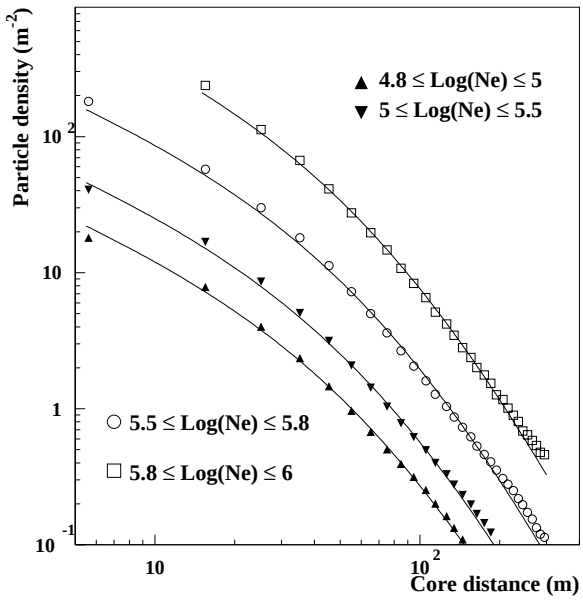

Fig. 2. Experimental average lateral distributions in different intervals of shower size and their fits to the NKG formula. The solid lines represent NKG *ldfs* with $s = 1.21$.

and linearity up to 400 particles m^{-2}. The time resolution, for single particles, is $\Delta t < 1.4$ ns.

Event selection for the present analysis requires at least 6 (or 7) modules fired (with threshold, for each module, set at 1/3 of the signal due to a minimum ionizing particle) and the highest particle density recorded by an inner detector, i.e. a detector not located at the edges of the array. Arrival directions are obtained from the time of flight technique with an accuracy, for the quoted events, of $\sigma_\theta = 0.83^\circ$ that improves to $\sigma_\theta = 0.5^\circ$ for events with $N_e > 10^5$.

The core location, the slope (s) of the lateral distribution function (*ldf* in the following) and the shower size are measured by means of a minimum χ^2 fit to the theoretical NKG *ldf* [13],

$$\rho(r) = N_e \frac{C(s)}{r_0^2}\left(\frac{r}{r_0}\right)^{s-2}\left(1+\frac{r}{r_0}\right)^{s-4.5} \text{ m}^{-2} \quad (2)$$

with normalization factor $C(s) = 0.366s^2(2.07 - s)^{1.25}$, and Molière radius $r_0 = 100$ m.

To check the NKG formula fit to the experimental data, average *ldfs* have been measured in different size intervals. Fig. 2 shows the results of such measurements and of their fits through expression (2): the agreement is good in every size interval; maximum differences are within 10% for large core distances.

The accuracy in the measurement of the shower size has been obtained by analyzing simulated data, including the experimental dispersion (1). The dependence of $\Delta N_e/N_e$ with N_e is shown in Fig. 3, being $\sim 10\%$ in the region of interest for the present analysis. The whole reconstruction procedures and accuracies are fully discussed in Ref. [12].

The consequences of possible inaccuracies of the NKG *ldf* on the determination of N_e and s have been investigated, using both a different value of r_0, as suggested in Ref. [14], and a modified *ldf* [2]. The maximum systematic differences are: $\Delta s < 0.2$ and $\Delta N_e/N_e < 6\%$. The maximum systematic uncertainty in the determination of N_e, due to the differences between the measured *ldf* and the theoretical NKG formula (see Fig. 2), is $\Delta N_e/N_e < 3\%$.

The analysis is performed in units of vertical minimum ionizing particles (*m.i.p.*, whose mean energy loss in the scintillator is 8.23 MeV), obtained experimentally, for calibrations, from single particle spectra (measured triggering each module in single mode). The shower size expressed in units of *m.i.p.* (Ne_{mip}) is converted to total number of charged particles (N_e, defined as the number of charged particles with en-

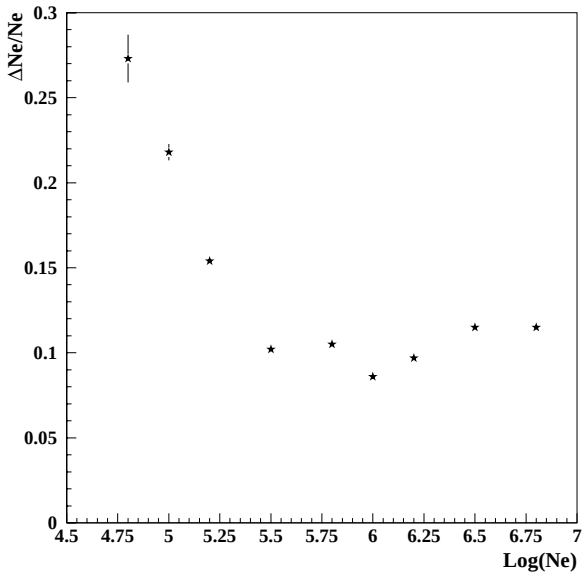

Fig. 3. Accuracy ($\Delta N_e/N_e$) in the determination of the shower size vs N_e. Events have been simulated with zenith angle θ between 0° and 40°; no dependence of the reconstruction accuracy on θ is observed in such range.

ergy $E > 0$ following Greisen expression [15]) taking into account the transition effect in the scintillators. This has been studied by means of simulations of the shower development in the atmosphere, in the detectors and in their housing, based on the GEANT code [16]. Further, it has been verified by means of a test performed, with the same scintillators and electronics operating on the field, at a CERN positron beam up to E_{e^+} = 50 GeV. Up to zenith angle θ = 40° the relation between Ne_{mip} and N_e is $N_e = Ne_{mip}/1.18$.

The trigger efficiency has been studied by simulating the array response as a function of zenith angle (θ) and shower size (including all experimental dispersions and triggering conditions). For events with core inside the fiducial areas (a) or (b) (referring to Fig. 1 for data acquired during runs (I) or (II)–(IV)) and $N_e > 10^{5.2}$, the trigger efficiency is greater than 95%, independent of θ (for $\theta < 40°$). All further analysis will therefore involve only events with $N_e > 10^{5.2}$ and core inside these areas; fluxes are corrected for the calculated trigger inefficiency.

Using the same simulation, the distortions of the shower size spectrum introduced by the event reconstruction have been studied. A trial spectrum (I_{mc} = number of events inside 12% size bins) generated with a unique power law index is compared with the spectrum resulting from the whole data processing (I_{ex} = number of events reconstructed in the quoted size bin). I_{mc}/I_{ex} does not appreciably depend on the slope of the trial spectrum (for $2.7 < \gamma < 3.1$) and its variation with N_e is

$$\frac{I_{mc}}{I_{ex}} = 0.934 + 0.148 \log \frac{N_e}{10^6} - 0.106 \log^2 \frac{N_e}{10^6}. \quad (3)$$

This expression is used to correct each bin content of the measured spectrum. The accuracy of the whole procedure allows us to obtain a measurement of the differential flux with systematic effects, due to the reconstruction procedure, not larger than 3%.

For the present analysis 256 days lifetime are used (corresponding $\approx 1.4 \times 10^7$ events). The dead time due to the data acquisition is 6%. Only events with $\theta < 40°$ and core falling inside the quoted fiducial areas (1.1×10^4 m^2 for run (I) and 2.5×10^4 m^2 for runs (II)–(IV)) are used in the analysis (for a total of 2×10^6 events).

3. Results

3.1. The size spectrum

To obtain the measurement of the absorption mean free path of showers in atmosphere the usual "constant intensity cut" technique [2] is followed. The measured absorption curve of EAS in atmosphere is fitted with an exponential law (x = atmospheric depth at zenith angle θ, and x_0 = 820 g cm^{-2} vertical depth corresponding to the average measured pressure),

$$N_e(\theta) = N_e(0°)\, e^{-(x-x_0)/\Lambda_e} = N_e(0°)\, e^{-(x_0/\Lambda_e)(\sec\theta - 1)}, \quad (4)$$

with $\overline{\Lambda_e}$ = 219 ± 3 g cm^{-2} (weighted mean of Λ_e calculated between intensities 2×10^{-7} and 10^{-6} m^{-2} s^{-1} sr^{-1}).

Fig. 4 and Table 1 show the differential size spectra measured in six different intervals of zenith angles; in Fig. 4 the spectra are multiplied by $N_e^{2.5}$ to emphasize the change of slope at the knee. The angular bin width is $\Delta \sec\theta = 0.05$. With such choice the maximum difference of atmospheric depth inside the same

Table 1
Values of the differential shower size (N_e) spectra measured in different intervals of zenith angle; the reported values are in units of 10^{-8} m^{-2} s^{-1} sr^{-1} N_e^{-1}

log N_e	$\Delta \sec\theta$ 1.00–1.05	$\Delta \sec\theta$ 1.05–1.10	$\Delta \sec\theta$ 1.10–1.15	$\Delta \sec\theta$ 1.15–1.20	$\Delta \sec\theta$ 1.20–1.25	$\Delta \sec\theta$ 1.25–1.30
5.20	50.76 ± 0.35	38.02 ± 0.32	28.68 ± 0.30	21.28 ± 0.28	15.73 ± 0.25	11.51 ± 0.23
5.25	42.64 ± 0.32	31.77 ± 0.29	23.60 ± 0.27	17.42 ± 0.25	13.29 ± 0.23	9.63 ± 0.21
5.30	34.95 ± 0.28	26.30 ± 0.27	19.87 ± 0.25	14.91 ± 0.23	11.07 ± 0.21	8.08 ± 0.19
5.35	28.93 ± 0.26	21.93 ± 0.24	16.35 ± 0.22	12.17 ± 0.21	9.05 ± 0.19	6.73 ± 0.17
5.40	24.03 ± 0.23	18.35 ± 0.22	13.86 ± 0.20	10.33 ± 0.19	7.72 ± 0.17	5.66 ± 0.16
5.45	20.08 ± 0.21	15.28 ± 0.20	11.45 ± 0.18	8.73 ± 0.17	6.35 ± 0.16	4.71 ± 0.15
5.50	16.87 ± 0.19	12.81 ± 0.18	9.65 ± 0.17	7.29 ± 0.16	5.31 ± 0.14	3.91 ± 0.13
5.55	14.10 ± 0.18	10.77 ± 0.17	7.79 ± 0.15	5.93 ± 0.14	4.45 ± 0.13	3.41 ± 0.12
5.60	11.75 ± 0.16	9.22 ± 0.15	6.71 ± 0.14	5.18 ± 0.13	3.63 ± 0.12	2.70 ± 0.11
5.65	9.97 ± 0.15	7.63 ± 0.14	5.63 ± 0.13	4.31 ± 0.12	3.13 ± 0.11	2.28 ± 0.10
5.70	8.49 ± 0.14	6.38 ± 0.13	4.74 ± 0.12	3.48 ± 0.11	2.59 ± 0.10	1.78 ± 0.09
5.75	6.88 ± 0.12	5.50 ± 0.12	4.08 ± 0.11	2.87 ± 0.10	2.06 ± 0.09	1.49 ± 0.08
5.80	5.76 ± 0.11	4.53 ± 0.11	3.36 ± 0.10	2.40 ± 0.09	1.72 ± 0.08	1.25 ± 0.07
5.85	4.86 ± 0.10	3.82 ± 0.10	2.73 ± 0.09	2.17 ± 0.08	1.46 ± 0.07	1.02 ± 0.07
5.90	4.11 ± 0.09	3.00 ± 0.09	2.29 ± 0.08	1.63 ± 0.07	1.25 ± 0.07	0.85 ± 0.06
5.95	3.34 ± 0.08	2.57 ± 0.08	2.03 ± 0.08	1.43 ± 0.07	1.02 ± 0.06	0.62 ± 0.05
6.00	2.90 ± 0.08	2.10 ± 0.07	1.54 ± 0.07	1.12 ± 0.06	0.84 ± 0.06	0.54 ± 0.05
6.05	2.39 ± 0.07	1.73 ± 0.07	1.28 ± 0.06	0.92 ± 0.06	0.71 ± 0.05	0.45 ± 0.04
6.10	1.90 ± 0.06	1.39 ± 0.06	1.03 ± 0.05	0.80 ± 0.05	0.53 ± 0.04	0.35 ± 0.04
6.15	1.63 ± 0.06	1.13 ± 0.05	0.83 ± 0.05	0.62 ± 0.04	0.41 ± 0.04	0.28 ± 0.03
6.20	1.17 ± 0.05	0.93 ± 0.05	0.66 ± 0.04	0.46 ± 0.04	0.33 ± 0.04	0.21 ± 0.03
6.25	0.97 ± 0.05	0.76 ± 0.04	0.52 ± 0.04	0.43 ± 0.04	0.29 ± 0.03	0.19 ± 0.03
6.30	0.82 ± 0.04	0.63 ± 0.04	0.43 ± 0.03	0.33 ± 0.03	0.20 ± 0.03	0.14 ± 0.02
6.35	0.65 ± 0.04	0.46 ± 0.03	0.36 ± 0.03	0.26 ± 0.03	0.16 ± 0.02	0.11 ± 0.02
6.40	0.49 ± 0.03	0.36 ± 0.03	0.29 ± 0.03	0.18 ± 0.02	0.12 ± 0.02	0.12 ± 0.02
6.45	0.39 ± 0.03	0.28 ± 0.03	0.22 ± 0.02	0.16 ± 0.02	0.10 ± 0.02	0.08 ± 0.02
6.50	0.31 ± 0.03	0.22 ± 0.02	0.17 ± 0.02	0.08 ± 0.02	0.08 ± 0.02	0.05 ± 0.01
6.55	0.23 ± 0.02	0.17 ± 0.02	0.14 ± 0.02	0.09 ± 0.02	0.08 ± 0.02	0.04 ± 0.01
6.60	0.19 ± 0.02	0.14 ± 0.02	0.10 ± 0.02	0.06 ± 0.01	0.04 ± 0.01	0.03 ± 0.01
6.65	0.15 ± 0.02	0.12 ± 0.02	0.08 ± 0.01	0.06 ± 0.01	0.04 ± 0.01	0.03 ± 0.01

bin is 40 g cm^{-2} (i.e., about one radiation length). The spectra refer to the depth corresponding to the mean zenith angle of the showers recorded inside each interval. The maximum difference in shower size, inside the same angular bin, using the measured value of Λ_e, is 17%.

The shapes of the spectra are very similar, the change of slope is seen at all zenith angles, at a size value $Ne_k(\theta)$ shifting as expected with zenith angle (i.e., atmospheric depth).

The behaviour of the parameters of the size spectrum versus atmospheric depth are studied fitting the experimental data with the following expression:

$$I(N_e,\theta) = I_k(\theta)\left(\frac{N_e}{Ne_k(\theta)}\right)^{-\gamma_{1,2}(\theta)}, \qquad (5)$$

γ_1 below, γ_2 above the knee[2].

Since all spectra have closely similar slopes below the knee (see Table 2), in the following γ_1 will no longer be fitted, in order to obtain a better accuracy on others parameters. The value of γ_1 calculated as weighted mean of the six individual values is

$$\gamma_1 = 2.56 \pm 0.02\,.$$

[2] All given errors on the parameters of the fits are calculated using the extreme parameter value corresponding to a χ^2 variation with respect to the minimum one $\Delta\chi^2/d.o.f. = 1$.

Table 2
Results obtained from the fits to the spectra measured in different bins of zenith angle. The third column reports the values of γ_1 obtained from the 4-parameter independent fits at all zenith angles, showing constancy of γ_1. Columns 4–6 show the results of the 3-parameter fits performed with a constant value of γ_1. The last column reports the slopes γ_2 obtained with the fit in which a constant integral flux above the knee is imposed.

$\Delta \sec\theta$	$\overline{x}$ (g cm^{-2})	γ_1	γ_2 (1st fit)	$I(>Ne_k)\times 10^7$ (m^{-2} s^{-1} sr^{-1})	$Log(Ne_k)$	γ_2 (2nd fit)
1.00–1.05	835	2.56 ± 0.02	2.99 ± 0.09	(0.99 ± 0.2)	6.09 ± 0.05	3.12 ± 0.05
1.05–1.10	880	2.55 ± 0.02	2.93 ± 0.11	(1.01 ± 0.3)	6.02 ± 0.07	2.92 ± 0.05
1.10–1.15	920	2.55 ± 0.03	2.85 ± 0.12	$(0.9.3 \pm 0.4)$	5.97 ± 0.08	2.87 ± 0.06
1.15–1.20	960	2.56 ± 0.03	2.81 ± 0.16	(0.80 ± 0.4)	5.93 ± 0.14	2.76 ± 0.06
1.20–1.25	1000	2.59 ± 0.03	2.91 ± 0.26	(0.52 ± 0.3)	5.95 ± 0.11	2.77 ± 0.07
1.25–1.30	1040	2.55 ± 0.07	2.80 ± 0.11	(1.30 ± 0.6)	5.63 ± 0.12	2.96 ± 0.08

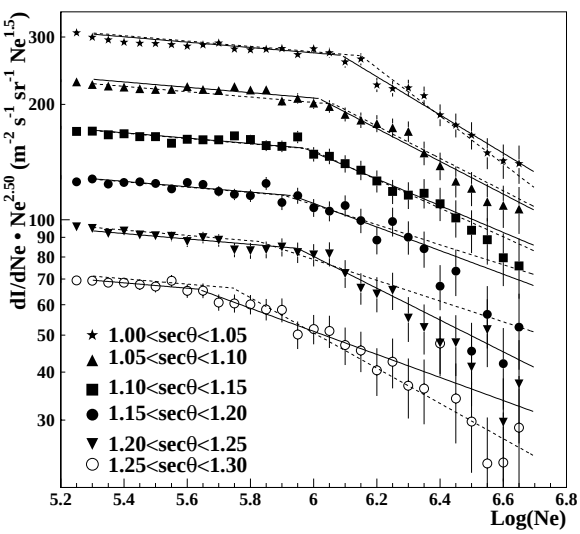

Fig. 4. Differential shower size spectra measured at different atmospheric depths. The solid lines show the results of the fitting procedure with 3 free parameters per spectrum, dashed lines those of the procedure requiring constant integral flux above the knee.

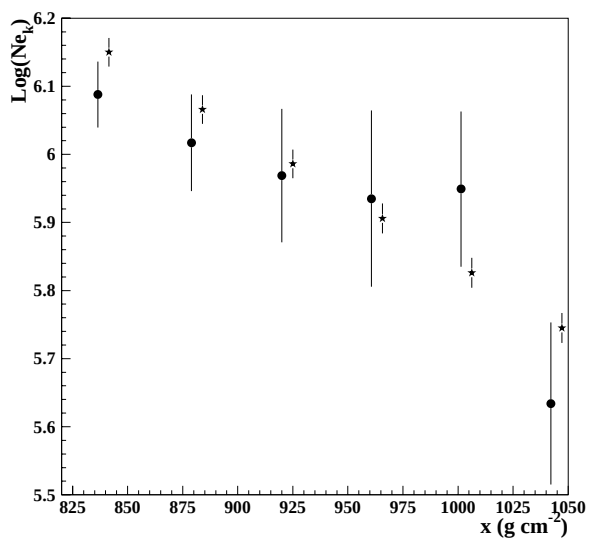

Fig. 5. Dependence of the size value of the knee on the atmospheric depth. Black dots show the results obtained fitting each spectrum independently, stars (shifted of Δx = 5 g cm^{-2}) those obtained under the physical hypothesis of a knee occurring at fixed primary energy. The two results are compatible inside the experimental uncertainties.

The results of the fits of each spectrum with free parameters, γ_2, Ne_k and I_k, are shown in Table 2, and, as Ne_k is concerned, in Fig. 5.

The shower size at the knee Ne_k decreases with increasing atmospheric depth, its attenuation length is $\Lambda_k = 257 \pm 80$ g cm^{-2}, while the intensity $I(>Ne_k)$ is constant inside experimental errors of $\approx 20\%$, a hypothesis which is verified with a $\chi^2 = 0.5/d.f.$

These data support a "normal" behaviour of showers at the 'knee' concerning the absorption in atmosphere and the integral intensity at different atmospheric depths (as should be for an effect occurring at a given primary energy).

Such hypothesis has been further introduced in the fit of the different spectra, requiring at the knee (for different zenith angles) constant integral flux ($I(>Ne_k) = (I_k Ne_k)/(\gamma_2 - 1)$), and shower size ($Ne_k$) attenuating exponentially with atmospheric depth. In this frame the free parameters are $Ne_k(0^\circ)$, $I(>Ne_k)$, Λ_k and the slopes γ_2 above the knee.

The obtained values are $I(>Ne_k) = (8.1 \pm 0.7) \times 10^{-8}$ m^{-2} s^{-1} sr^{-1}, $Ne_k(0^\circ) = 10^{6.15 \pm 0.02}$, and $\Lambda_k = 222 \pm 3$ g cm^{-2}, a value which is in excellent agreement with the attenuation length obtained for EAS

particles from the constant intensity cut technique.

Concerning Ne_k, the results are shown in Fig. 5. We observe that the values of Ne_k at every atmospheric depth are compatible, within the experimental errors, with the results of the previous fit.

The results of the fit concerning γ_2 are also reported in Table 2. An indication of a decrease of γ_2 with increasing zenith angle is derived: its compatibility with a constant value is excluded with a $\chi^2 \approx 5.86/d.f.$; i.e. a chance probability of $\sim 2 \times 10^{-5}$. This is expected due to the attenuation of showers with increasing atmospheric depth. A similar variation is however not observed below the 'knee' for γ_1: such effects need to be further investigated with improved statistics, and possibly correlated with the spectra of other components (e.g., muons).

3.2. The energy spectrum

The conversion from primary energy (E_0) and mass (A) to shower size (N_e) has been obtained by means of complete simulations of the cascades in atmosphere using the CORSIKA-HDPM code [17]. The mean conversion from primary energy (E_0, in TeV) to shower size (N_e in Greisen formalism, as for the experimental data) at the depth of 810 g cm^{-2} (i.e., the standard pressure corresponding to 2000 m a.s.l.), obtained simulating sets of events at fixed primary energies, is

$$N_e(E_0, A) = \alpha(A) E_0^{\beta(A)}, \tag{6}$$

where $\alpha(A) = 197.5A^{-0.521}$ and $\beta(A) = 1.107A^{0.035}$.

Fluctuations are

$$\frac{\sigma(N_e)}{N_e} = \kappa(A) E_0^{-\xi(A)}, \tag{7}$$

where $\kappa(A) = 1.495A^{-0.197}$ and $\xi(A) = 0.249 \times A^{-0.056}$.

The effects on the size spectra of such fluctuations in the EAS development have been taken into account simulating events on a trial power law energy spectrum for primary protons. The shower size spectrum ($I_{\rm mc}$) resulting from the mean conversion (6) and the one ($I_{\rm fl}$) calculated including fluctuations (7) are compared ($I_{\rm mc}$ and $I_{\rm fl}$ represent the number of counts in 12% shower size bins). The resulting correction is

$$\frac{I_{\rm mc}}{I_{\rm fl}} = 0.959 + 0.051 \log \frac{N_e}{10^6} - 0.021 \log^2 \frac{N_e}{10^6}. \tag{8}$$

This function depends on the index γ of the spectrum, events are therefore generated on a trial spectrum reproducing the measured one.

The all particle energy spectrum is obtained, from all events with $\theta < 40^\circ$, converting every shower size to 810 g cm^{-2} using the measured absorption length ($\Lambda_e = 219 \pm 3$ g cm^{-2}). The effective value of the primary mass (to be used in expression (6)) is calculated from the extrapolation of the single nuclear spectra ($\Phi_i = b_i \cdot E_o^{-\gamma_i}$) measured at lower energies by experiments operating at the top of the atmosphere (JACEE Collaboration [18] for the light elements, CRN [19] for the heavier ones),

$$A_{\rm eff}(N_e) = \frac{\sum_i A_i \Phi_i(N_e)}{\sum_i \Phi_i(N_e)}. \tag{9}$$

The value of $A_{\rm eff}$ above the knee is calculated using a rigidity dependent cutoff: $E_k(A) = Z \cdot 2 \cdot 10^{15}$ eV, and $\gamma_i \Rightarrow \gamma_i + 0.4$ for $E_o > E_k(A)$ and all nuclear mass groups ($A_{\rm eff}$ changes from 7.1 at $N_e = 10^{5.2}$, to 8.9 at $N_e = 10^{6.0}$ and 10.9 at $N_e = 10^{6.5}$).

The validity of the extrapolation of the low energy composition data up to the knee is supported by the good agreement between the size spectrum calculated under such hypothesis and the measured one, as shown in Fig. 6. Further it agrees with the $N_e - N_\mu$ measurements both for $E_\mu > 1.4$ TeV [20] and for $E_\mu > 1$ GeV [21]. The $N_e - N_\mu$ data also support the rigidity dependent cutoff used to calculate the effective primary mass above the knee [20,22].

Fig. 7 shows the obtained intensity: below the knee it is well connected with the results of the experiments operating on balloon or satellites [23,24]; at the knee and above, the agreement between the EAS data [2,25,26] is quite good.

From power law fits to the energy spectrum performed below and above the knee we obtain, for 900 TeV $< E_0 <$ 2300 TeV,

$$S(E_0) = (3.48 \pm 0.06) \times 10^{-10} (E_0/2300)^{-2.76 \pm 0.03}\ \mathrm{m^{-2}\,s^{-1}\,sr^{-1}\,TeV^{-1}},$$

and for 5000 TeV $< E_0 < 10^4$ TeV,

$$S(E_0) = (3.77 \pm 0.08) \times 10^{-11} (E_0/5000)^{-3.19 \pm 0.06}\ \mathrm{m^{-2}\,s^{-1}\,sr^{-1}\,TeV^{-1}}.$$

The given errors are the statistical ones.

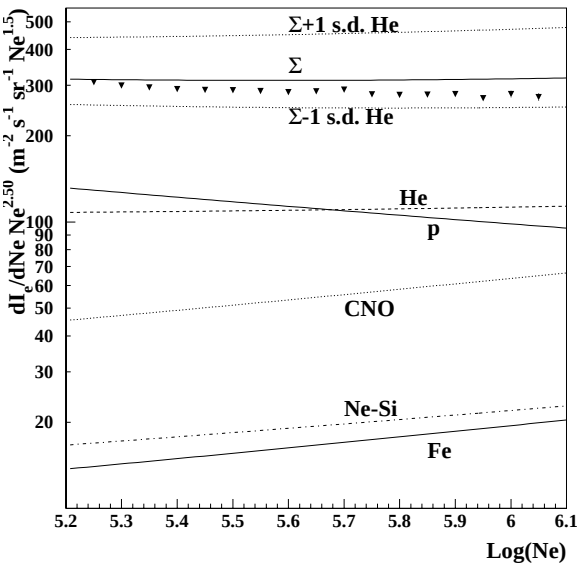

Fig. 6. Comparison of the shower size spectrum with the one expected (Σ) from the extrapolation of the low energies direct data (see text for references). The expectations which include the experimental errors on the helium flux ($\Sigma \pm 1$ *s.d.* He), and the contributions of the different primaries are also shown. Notice that the extrapolations of the direct data predict comparable contributions to the size spectrum at the knee from p and He primaries.

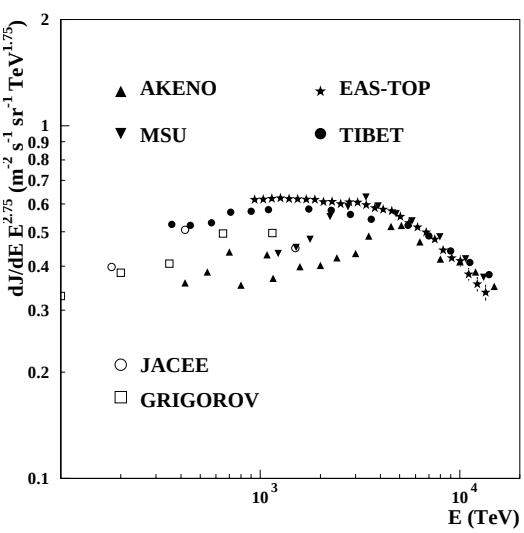

Fig. 7. The all particle spectrum obtained from the EAS-TOP shower size data, compared with the results of other experiments operating outside the atmosphere or at ground level (see text for references).

The systematic uncertainties in the energy spectrum due to the primary composition ($A_{\rm eff}$) and the hadronic interaction model used ($N_e(E_0, A)$) have been evaluated:

(a) one standard deviation errors (from direct measurements) of opposite signs have been applied to each "light" and "heavy" component in order to obtain "upper" and "lower" limits to $A_{\rm eff}$. The all particle spectrum, obtained in the "light" and "heavy" limits, still compatible with the direct measurements, differs of $\pm 10\%$ from the one calculated with the mean value of $A_{\rm eff}$ (reported in Fig. 7).

(b) The shower sizes obtained from different interaction models included in the CORSIKA code have been compared at $E_0 = 2 \times 10^{15}$ eV. The maximum difference in the determination of N_e between the tested models (namely, QGSJET, DPMJET, SIBYLL) and the reference one (HDPM) is also about 10%.

If the "knee" is due to the steepening of a single component, its corresponding energy, as obtained from the size spectrum, depends obviously on the mass number of such component. Following the extrapolations of the low energy data the component dominating the size spectrum at the knee energy should be a light one (p,He), or CNO [10]. The corresponding knee energies, obtained from the vertical value of Ne_k, are $E_k \approx (2.7\text{–}3.4\text{–}4.1) \times 10^{15}$ eV, respectively.

4. Conclusions

From the measurement of the size spectrum in the energy region $E_0 = 10^{15}$–10^{16} eV of the cosmic ray energy spectrum ("knee" region), we conclude:

(a) The size spectrum in the region below the knee agrees with the expectations obtained from the extrapolations of the direct measurements.

(b) At the atmospheric depth of 835 g cm^{-2} the "knee" is observed at $Ne_k = 10^{6.09 \pm 0.05}$, the corresponding intensity being $I(> Ne_k) = (9.9 \pm 2.1) \times 10^{-8}$ m^{-2} s^{-1} sr^{-1}, with a change of the index of the power law from $\gamma_1 = 2.56 \pm 0.02$ to $\gamma_2 = 2.99 \pm 0.09$.

(c) The break is "sharp", i.e., inside a few percent accuracies of the data, it can be represented by "two power laws" intersecting spectra. Of course

less "sharp" fits represent, inside the experimental uncertainties, the data as well, but, in any case, the change in slope has to occur in a rather "limited" range of N_e. This represents a constraint that has to be taken into account by any physical explanation of the "knee" and could be difficult to be explained by interpretations based on diffusion models, that imply "slow" variations of the spectra with primary energy [7].

(d) The shower size at the knee (Ne_k) attenuates with increasing atmospheric depth; its attenuation length is compatible with the attenuation of EAS particles in the same energy range.

(e) The energy corresponding to the knee is $E_k \approx (2.7\text{–}3.4\text{–}4.1) \times 10^{15}$ eV for proton, Helium and CNO primaries respectively. Power laws fits to the energy spectrum below and above the knee give

$$S(E_0) = (3.48 \pm 0.06) \times 10^{-10} (E_0/2300)^{-2.76\pm0.03} \ \mathrm{m^{-2}\ s^{-1}\ sr^{-1}\ TeV^{-1}}$$

for 900 TeV $< E_0 <$ 2300 TeV and

$$S(E_0) = (3.77 \pm 0.08) \times 10^{-11} (E_0/5000)^{-3.19\pm0.06} \ \mathrm{m^{-2}\ s^{-1}\ sr^{-1}\ TeV^{-1}}$$

for 5000 TeV $< E_0 < 10^4$ TeV.

Systematic uncertainties are $\pm 10\%$ both due to the uncertainties in composition and in hadronic interaction models.

Acknowledgements

The continuous cooperation of the Director and of the Staff of the Gran Sasso National Laboratories, as well as the technical assistance of C. Barattia, M. Canonico, G. Giuliani and G. Pirali are gratefully acknowledged.

References

[1] G. Kulikov, G.B. Khristiansen, JEPT 35 (1958) 635.
[2] M. Nagano et al., J. Phys. G 10 (1984) 1295.
[3] G. Navarra et al., EAS-TOP Collaboration, Nucl. Phys. B (Proc. Suppl.) 60B (1998) 105.
[4] R. Glasstetter et al., KASKADE Collaboration, Proc. 25th ICRC, Vol. 6, Durban (1997) p. 157.
[5] O.A. Gress et al., Proc. 25th ICRC, Vol. 4, Durban (1997) p. 129.
[6] J. Cortina et al., HEGRA Collaboration, Proc. 25th ICRC, Vol. 4, Durban (1997) p. 69.
[7] B. Peters, Proc. 23rd ICRC, Vol. 3, Moskow (1959) 157; G.T. Zatsepin et al., Izv. Ak. Nauk USSR SP 26 (1962) 685.
[8] A.M. Hillas, Proc. 16th ICRC, Vol. 8, Kyoto (1970) p. 7.
[9] P.L. Biermann, Proc. 23rd ICRC, Vol. 45, Calgary, Invited, Rapporteur and Highlight papers (1994).
[10] A.D. Erlykin, A.W. Wolfendale, J. Phys. G. 23 (1997) 979; Astrop. Phys. 7 (1997) 1.
[11] EAS-TOP Collaboration, Proc 24th ICRC, Vol. 2, Roma (1995) p. 732;
EAS-TOP Collaboration, Proc. 25th ICRC, Vol. 4, Durban (1997) p. 125.
[12] M. Aglietta et al., Nucl. Instrum. & Methods A 336 (1993) 310.
[13] K. Kamata et al., Suppl. Progr. Theor. Phys. 6 (1958) 93.
[14] A.M. Hillas, Proc. 17th ICRC, Vol. 6, Paris (1981) p. 244.
[15] K. Greisen, Ann. Rev. Nucl. Sci. 10 (1960) 78.
[16] R. Brun et al., report CERN DD/EE/84-1 (1984).
[17] J.N. Capedevielle et al., The Karlsrhue Extensive Air Shower Simulation Code CORSIKA, Kernforschungszentrum Karlsrhue, KfK 4998 (1992).
[18] K. Asakimori et al., JACEE Collaboration, Proc. 22nd ICRC, Vol. 2, Dublin (1991) p. 57.
[19] D. Muller et al., Ap. J. 374 (1991) 356.
[20] M. Aglietta et al., EAS-TOP, MACRO Collaboration, Phys. Lett. B 337 (1994) 376;
EAS-TOP, MACRO Collaboration, Proc. 25th ICRC, Vol. 4, Durban (1997) p. 41.
[21] EAS-TOP Collaboration, Proc. 25th ICRC, Vol. 4, Durban (1997) p. 13.
[22] Yu.A. Fomin et al., J. Phys. G 22 (1996) 1839.
[23] N.L. Grigorov et al., Proc. 12th ICRC, Vol. 5, Hobart (1971) p. 1746.
[24] M. Ichimura et al., Proc. 22nd ICRC, Vol. 2, Calgary (1993) p. 5.
[25] Yu. A. Fomin et al., Proc. 22nd ICRC, Vol. 2, Dublin (1991) p. 85.
[26] Amenomori et al., The Tibet Asγ Collaboration, Ap. J. 461 (1996) 408.